Photosynthesis Research
https://doi.org/10.1007/s11120-023-01047-5

RESEARCH

A quantitative assessment of (bacterio)chlorophyll assignments in the cryo-EM structure of the *Chloracidobacterium thermophilum* reaction center

Christopher J. Gisriel[1] · David A. Flesher[2] · Zhuoran Long[1] · Jinchan Liu[2] · Jimin Wang[2] · Donald A. Bryant[3] · Victor S. Batista[1] · Gary W. Brudvig[1,2]

Received: 17 May 2023 / Accepted: 31 August 2023

Abstract
Chlorophylls and bacteriochlorophylls are the primary pigments used by photosynthetic organisms for light harvesting, energy transfer, and electron transfer. Many molecular structures of (bacterio)chlorophyll-containing protein complexes are available, some of which contain mixtures of different (bacterio)chlorophyll types. Differentiating these, which sometimes are structurally similar, is challenging but is required for leveraging structural data to gain functional insight. The reaction center complex from *Chloroacidobacterium thermophilum* has a hybrid (bacterio)chlorophyll antenna system containing both chlorophyll *a* and bacteriochlorophyll *a* molecules. The recent availability of its cryogenic electron microscopy (cryo-EM) structure provides an opportunity for a quantitative analysis of their identities and chemical environments. Here, we describe a theoretical basis for differentiating chlorophyll *a* and bacteriochlorophyll *a* in a cryo-EM map, and apply the approach to the experimental cryo-EM maps of the (bacterio)chlorophyll sites of the chloroacidobacterial reaction center. The comparison reveals that at ~ 2.2-Å resolution, chlorophyll *a* and bacteriochlorophyll *a* are easily distinguishable, but the orientation of the bacteriochlorophyll *a* acetyl moiety is not; however, the latter can confidently be assigned by identifying a hydrogen bond donor from the protein environment. This study reveals the opportunities and challenges in assigning (bacterio)chlorophyll types in structural biology, the accuracy of which is vital for downstream investigations.

Keywords Photosynthesis · Light harvesting · Chlorophyll · Bacteriochlorophyll · Cofactor assignment · Cone scan · Hydrogen bonding · *Chloracidobacterium thermophilum*

Introduction

The light reactions of photosynthesis employ membrane-intrinsic, pigment-protein complexes that convert the energy of sunlight into chemical potential energy. To achieve this, the protein complexes coordinate various pigments that are involved in light absorption, energy transfer, electron transfer, and energy dissipation. Chlorophyll (Chl) and bacteriochlorophyll (BChl) molecules (hereafter referred to collectively as "(bacterio)chlorophylls" [(B)Chls]) are the most important of these pigments, comprising most of the electron transfer cofactors and antenna molecules in Chl-dependent (chlorophototrophic) organisms, both oxygenic and anoxygenic (Blankenship 2021). (B)Chls are tetrapyrroles whose highly conjugated systems result in the ability to absorb photons in the ultraviolet, visible, and near-infrared regions of the solar spectrum. There are a variety of (B)Chl types (Bryant et al. 2020): Chls *a*, *b*, *c*, *d*, and *f*, and BChls *a*, *b*, *c*, *d*, *e*, and *g*. Additionally, there are derivatives of these, for example, 8^1-OH-Chl *a* found in the reaction center of bacterial species differs from the more common Chl *a* by an additional hydroxyl moiety (van de Meent et al. 1991). There are further variations in the identity of (B)Chl hydrocarbon

Christopher J. Gisriel and David A. Flesher contributed equally to this work.

✉ Gary W. Brudvig
gary.brudvig@yale.edu

[1] Department of Chemistry, Yale University, New Haven, CT 06520, USA

[2] Department of Molecular Biophysics and Biochemistry, Yale University, New Haven, CT 06520, USA

[3] Department of Biochemistry and Molecular Biology, The Pennsylvania State University, University Park, PA 16802, USA

Published online: 25 September 2023

tails. Many chlorophototrophs contain only a single type of (B)Chl, including most cyanobacteria that contain only Chl *a*. Other organisms contain a mixture of different (B)Chls, such as plants and green algae that produce both Chl *a* and Chl *b* or green sulfur bacteria like *Chlorobaculum tepidum* that produce three (B)Chls: BChl *a*, BChl *c*, and Chl *a* (Chew and Bryant 2007). The (B)Chl composition found in different chlorophototrophs varies because organisms have adapted to optimize their light-harvesting systems to absorb the light available in their growth environments (Bryant and Canniffe 2018). For example, diatoms contain both Chl *a* and Chl *c*, the latter of which strongly absorbs blue light that is enriched in aquatic environments (Strain and Manning 1942; Strain et al. 1943). In contrast, some terrestrial cyanobacteria contain a mixture of Chls *a*, *d*, and *f*, the latter two of which absorb far-red light that goes mostly unused by the Chl *a*- and Chl *b*-containing plants or other chlorophototrophs that may shade them (Gan et al. 2014a, b; Gan and Bryant 2015). Thus, the (B)Chl composition of chlorophototrophs is central to their ability to survive and compete in diverse light regimes.

To understand the structure–function relationships of the pigment–protein complexes described above, structural biologists have targeted their efforts at solving their molecular structures. Recent years have seen a boom in structural reports of (B)Chl-containing complexes due to the popularization and ease of the technique cryogenic electron microscopy (cryo-EM) (Kühlbrandt 2014). When experimentalists model (B)Chl molecules into the corresponding electrostatic potential maps, the situation is fairly simple if only a single (B)Chl type is present—there is no question as to which (B)Chl type should be modeled. The situation is complicated when multiple (B)Chl types are present in a molecular structure because the modeler must decide which type fits the map best. This often presents major challenges because the differences among (B)Chls are sometimes structurally minor, although the correct assignment can hold major significance for understanding how energy and electrons are transferred (Gisriel et al. 2020b). A prime example is given in the assignment of Chls *a* and *f* molecules in the structures of photosystem I expressed during far-red light photoacclimation (Gisriel et al. 2020a, 2021, 2022a; Kato et al. 2020). The only structural difference between Chl *a* and Chl *f* is that in Chl *a,* there is a methyl moiety at the C3 position of the tetrapyrrole ring, and for Chl *f,* there is a formyl moiety at the C3 position. The situation is additionally complicated by the fact that a cryo-EM map is an electrostatic potential map of the molecule; therefore, the map signal is diminished for negatively charged species (Wang and Moore 2017), such as the oxygen atom of the formyl moiety in the case of Chl *f* which carries a partial negative charge. Thus, the resolution requirement for directly differentiating Chl *a* from Chl *f* appears to be relatively high, ~ 2.5–3.0 Å, though a strict resolution cutoff is dependent on the dataset and the occupancy and mobility of specific (B)Chls (Gisriel et al. 2021). Fortunately, indirect evidence from the protein environment has proven useful for determining Chl *f* sites because H-bond donors (waters or protein) are almost always present near the C3 formyl group, lending evidence for sites binding Chl *f*. More recently, the ability to quantify cryo-EM maps and to assign more accurately (B)Chl types has been established. Namely, the "cone scan" method has been used to help determine which Chl type should be assigned in several far-red light-acclimated photosystem structures from multiple organisms (Gisriel et al. 2021, 2022a, b, 2023); however, in these structures, only a small number of the Chls are not Chl *a*, and the minor structural difference between Chls *a* and *f* makes it difficult to assess fully the capability of the cone scan method for quantitative analyses. An ideal system to evaluate the cone scan method further would be a high-resolution map containing a heterogenous mixture of (B)Chl types.

Recently, the cryo-EM structure of the reaction center complex from *Chloroacidobacterium thermophilum* was reported at a global resolution of 2.2 Å (Dong et al. 2022). Chloroacidobacteria are microaerophilic, anoxygenic photoheterotrophic prokaryotes (Bryant et al. 2007; Tank and Bryant 2015). Their reaction center complex, referred to here as CabRC, (He et al. 2019; Dong et al. 2022) contains a homodimeric core that binds 10 Chl *a* molecules, 16 BChl *a* molecules, and two Zn-BChl *a′* molecules (Fig. 1), the latter of which is identical to BChl *a* except that the central metal ion is Zn and there is reversed stereochemistry about the 13^2 carbon. The hybrid antenna system

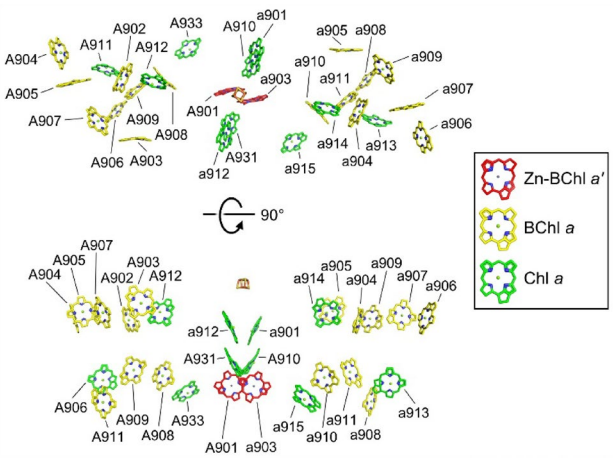

Fig. 1 Organization and assignment of (B)Chl sites from the CabRC. The tetrapyrrole rings only are shown and colored corresponding to the assignments made from the CabRC cryo-EM structure (Dong et al. 2022). The [4Fe-4S] cluster bound by the homodimeric core is additionally shown for orientation (colored orange and yellow). Sites are labeled with their chain (letter) and number based on the molecular coordinates (Protein Data Bank [PDB] 7VZR)

comprises 6 of the Chl *a* molecules and all 16 BChl *a* molecules (Tsukatani et al. 2012; He et al. 2019; Dong et al. 2022), and the electron transport chain cofactors comprise the two Zn-BChl *a′* molecules, which form the special pair P_{840} (Charles et al. 2020; Dong et al. 2022) and four of the Chl *a* molecules, two of which have been shown to be primary electron acceptors (Zill et al. 2018; Dong et al. 2022). The differences between Chl *a* and BChl *a*, shown in Fig. 2, are that (a) the C3 position of Chl *a* contains a vinyl moiety whereas the C3 position of BChl *a* contains an acetyl moiety, and (b) the unsaturation of ring B in BChl *a* causes the C7 and C8 carbons to be chiral centers whereas both of those carbon positions exhibit a planar geometry in Chl *a*. Because of these relatively major differences, the assignment of the (B)Chl types in the cryo-EM map is likely to be trustworthy at the resolution achieved. This provides an opportunity for the CabRC structural data to serve as a system to benchmark a quantitative analysis of (B)Chl type assignments in a cryo-EM map.

Here, we generated theoretical electrostatic potential maps (i.e., cryo-EM maps) of Chl *a* and BChl *a* at the same resolution as the recent CabRC structure. The cone scan method reported previously (Gisriel et al. 2021) was employed to predict what features of the map an experimentalist might expect in a quantitative analysis of (B)Chl sites. The theoretical expectations are compared to cone scans of the experimental data, and the protein environment is additionally assessed. The data provide a blueprint for (B)Chl assignment useful for molecular structures that contain mixtures of (B)Chl types.

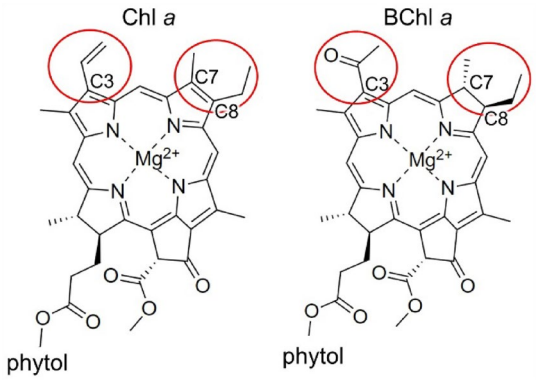

Fig. 2 Molecular structures of Chl *a* and BChl *a*. Red circles highlight the major structural differences between the two (B)Chl

Materials and methods

(B)Chl structure optimization and calculated electrostatic potentials

Chl *a* and BChl *a* were taken from PDB 7VZR (cofactor names and numbers CLA910 and BCL905, respectively). The structures were optimized with the Gaussian 16 software package (Frisch et al. 2016, p. 16) using density functional theory with the B3LYP functional (Becke 1993) and the 6-31G(d,p) (Ditchfield et al. 1971; Hehre et al. 1972; Hariharan and Pople 1973) basis set. To obtain electron density and electrostatic potential distributions for cone scans, single point calculations were performed with optimized structures using the same functional and basis set.

Cone scan analysis

Cone scans on both the theoretical and experimental maps were performed as described previously with minor modifications (Gisriel et al. 2021). The map for each (B)Chl molecule was aligned to a reference Chl using the tetrapyrrole ring only and inverted using CCP4 (Winn et al. 2011), Rave (Kleywegt and Jones 1994), and Phenix (Adams et al. 2010). Maps were scaled and extracted over 360° at intervals of 5° for each specified bond distance. Heat maps were generated by extracting map data across a range of bond distances. The files and corresponding code used to generate these data are included as Supplementary Data 1.

Structural analysis and multiple sequence alignment

For structural analysis, PDB model 7VZR and its corresponding map, EMD-32229, were used. To alter the orientation of the BChl *a* molecules in sites A902, A906, and a908, the map, model, and restraints (ligand BCL in the PDB) were loaded into Coot version 0.9.8.1 (Emsley et al. 2010) and locally refit. A coordinate file containing these changes is included as Supplementary Data 2. The multiple sequence alignment was generated using Clustal Omega (Sievers et al. 2011).

Results

Density functional theory-derived electrostatic potential maps and cone scans.

To provide a theoretical basis for quantifying the distinction between Chl *a* and BChl *a*, we generated their electrostatic

potential maps and smoothed them to a B-factor equivalent to 2.2-Å resolution (top panels of Fig. 3) as described in Sect. "Materials and Methods". This resolution was chosen because it is the same as the global resolution of the experimental CabRC structure (Dong et al. 2022). The cone scan method was used to create a heat map of the signal from the theoretical map in a cone extending away from $C3^1$ (middle panels of Fig. 3). Heat maps and cone scans corresponding to 2.0-, 2.5-, 3.0-, and 3.5-Å resolutions are additionally shown in Supplementary Fig. 1 and Supplementary Fig. 2, respectively. In heat maps of the Chl *a* C3 vinyl moiety, a single primary peak is observed in the direction at which it is modeled in the optimized structure, ~ 30°. At 2.2 Å resolution, another much smaller peak is also present that arises from the $C3^1$ H-atom, although this feature is mostly lost at lower resolutions (Supplementary Fig. 1). In heat maps of the BChl *a* C3 acetyl moiety, two peaks are observed at ~ 0/360° and 180°. Although the peaks are similar in height and amplitude, the peak arising from the methyl group is larger than that arising from the carbonyl

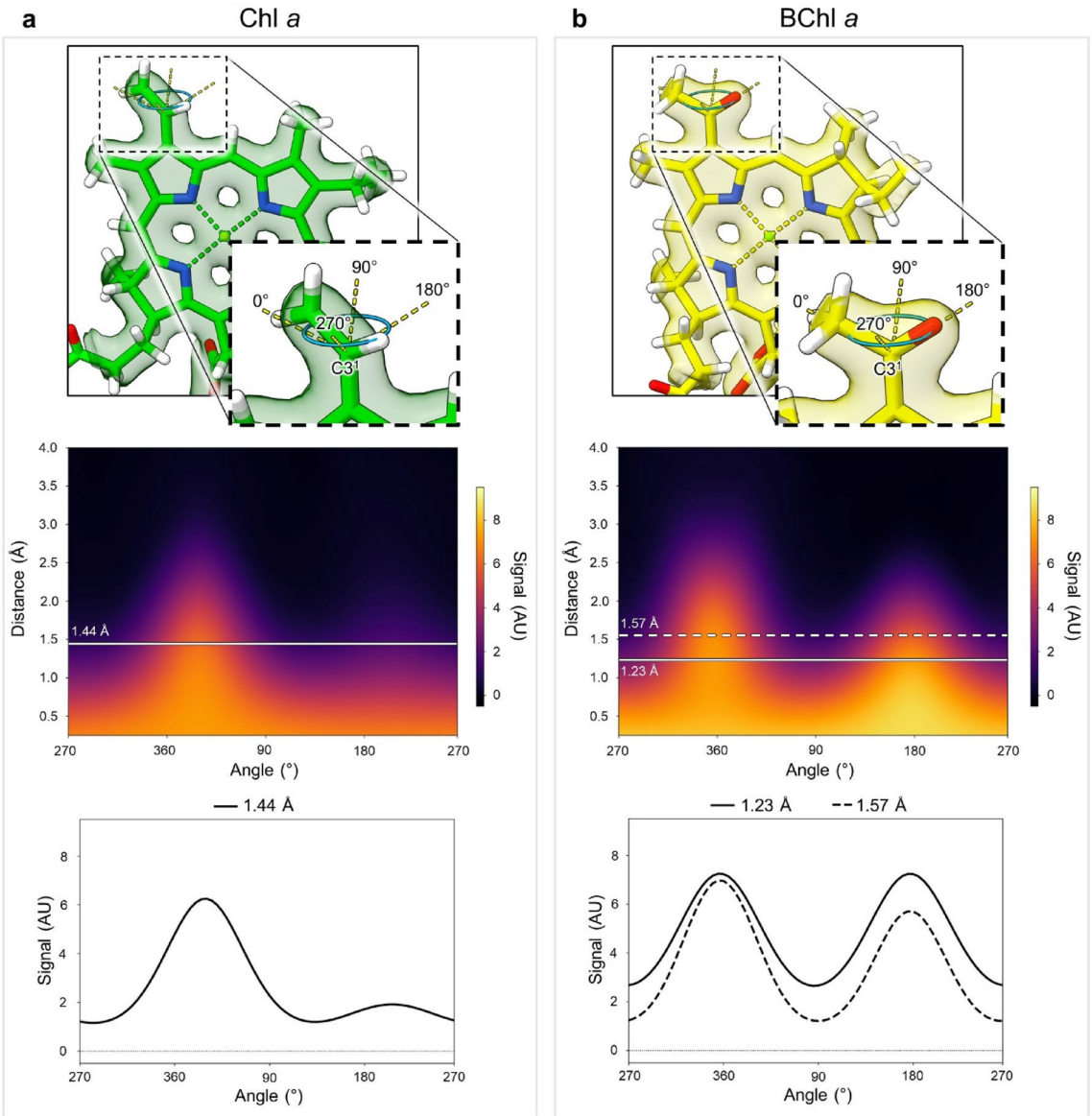

Fig. 3 Theoretical cone scans of the C3 position on Chl *a* and BChl *a*. Panel **a** shows the data for Chl *a* and panel **b** shows the data for BChl *a*. Top: The (B)Chl in its corresponding calculated 2.2-Å resolution map. The inset shows the C3 position and an example cone scan used for the data below it. Middle: Heat maps of cone scans moving away from the $C3^1$ carbon atom (*Y* axis). For panel **a**, the horizontal line is shown at a distance of 1.44 Å which is the optimal distance of a C = C bond. For panel **b**, the horizontal lines are shown at distances of 1.23 Å and 1.57 Å which are the optimal distances of C = O and C − C bonds, respectively. Bottom: Cone scans generated from the horizontal lines shown in the middle panels

group. Cone scans were extracted at distances corresponding to expected bond distances: 1.44 Å for the C=C bond of the vinyl moiety of Chl *a*, and 1.23 Å and 1.57 Å for the C=O and C−C bonds of the acetyl moiety of BChl *a*, respectively (bottom panels in Fig. 3). These cone scans neatly capture the single-peak profile for the C3 vinyl moiety of Chl *a* and the two-peak profile of the C3 acetyl moiety of BChl *a*. In the latter, the peak amplitudes of the 1.23 Å scan are approximately equal, but in the 1.57 Å scan, they are more distinct due to the steep drop-off of the signal from the carbonyl at the increased distance.

Structural validation

The CabRC structure was solved to 2.2-Å resolution, which is relatively high compared to most other (B)Chl-containing cryo-EM structures. Although properly assigning (B)Chl types can be challenging (Gisriel et al. 2020b), the differences between Chl *a* and BChl *a* (Fig. 2) should be easily distinguished at ~2.2-Å resolution. Furthermore, the oxygen of the C3 acetyl moiety of BChl *a* most likely serves as an H-bond acceptor, as is the case for chlorophylls *b*, *d*, and *f* (Gisriel et al. 2020a, b, 2021, 2022b). Prior to comparing the theoretical cone scan data to experimental cone scans, we assessed the deposited structure and map by visual inspection to ensure the assignments were correct. None of the cryo-EM map regions corresponding to the C3 positions of Chl *a* or BChl *a* suggested an incorrect assignment. Furthermore, the map corresponding to all of the C7 and C8 positions for Chl *a* appeared to exhibit planar geometries and for BChl *a* (and Zn-BChl *a'*) exhibited tetrahedral geometries (Supplementary Fig. 3). These observations support the modeled (B)Chl types originally assigned (Dong et al. 2022).

We also verified the H-bonding interactions of the BChl *a* and Zn-BChl *a'* acetyl moieties. Of the 18 BChl *a* or Zn-BChl *a'* molecules, 11 exhibit H-bond donors to the oxygen atom of the C3 acetyl moiety in the deposited coordinates. The seven that do not are in sites A901, a903, A902, A906, a908, A907, and a909. A901 and a903 are the pair of Zn-BChl *a'* molecules that comprise P_{840}. Although no H-bond donor to the acetyl moieties was present in the originally deposited coordinates, the map clearly shows signals for water molecules that donate H-bonds to the carbonyl groups (Fig. 4). Each water molecule also donates an H-bond to the 13^2-methoxycarbonyl substituent of the other BChl *a'* in P_{840} and accepts an H-bond from the sidechain of PscA-Tyr856. Notably, the signals of the central metal ions in P_{840} are greater than those observed for nearby (B)Chl molecules, supporting their assignment as Zn-BChl *a'* (Supplementary Fig. 4) (Charles et al. 2020). The BChl *a* molecule in site A902 has its C3 acetyl moiety in an unlikely configuration: its methyl group is positioned in a polar environment and its carbonyl oxygen in a hydrophobic environment (Fig. 5). It is more likely that the correct orientation should be flipped. When this is modeled in this manner, the carbonyl oxygen is within H-bonding distance of PscA-His307, likely accepting an H-bond from this residue. It should also be noted that the BChl *a* in site A902 is related by symmetry with that in site a904 (Fig. 1), and the acetyl moiety of a904 is correctly modeled in the originally deposited coordinates.

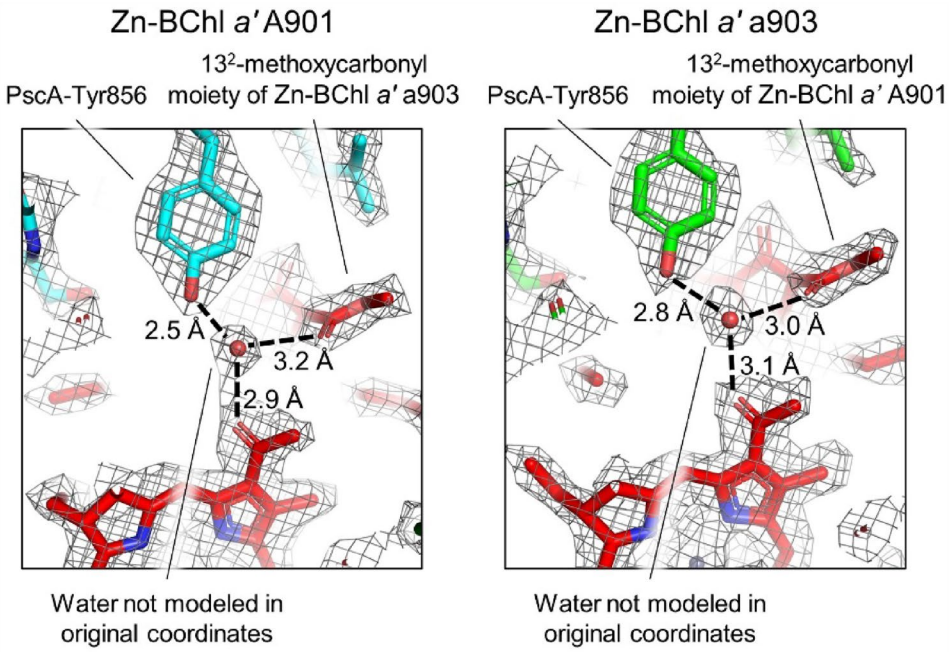

Fig. 4 Water H-bonding to the C3 acetyl moieties of the Zn-BChl *a'* molecules in sites A901 and a903 (P_{840}). The structure within the originally deposited map is shown and a water molecule is additionally modeled within H-bonding distance of the carbonyl group of the C3 acetyl moiety, PscA-Tyr856, and the adjacent molecule's 13^2-methoxycarbonyl moiety

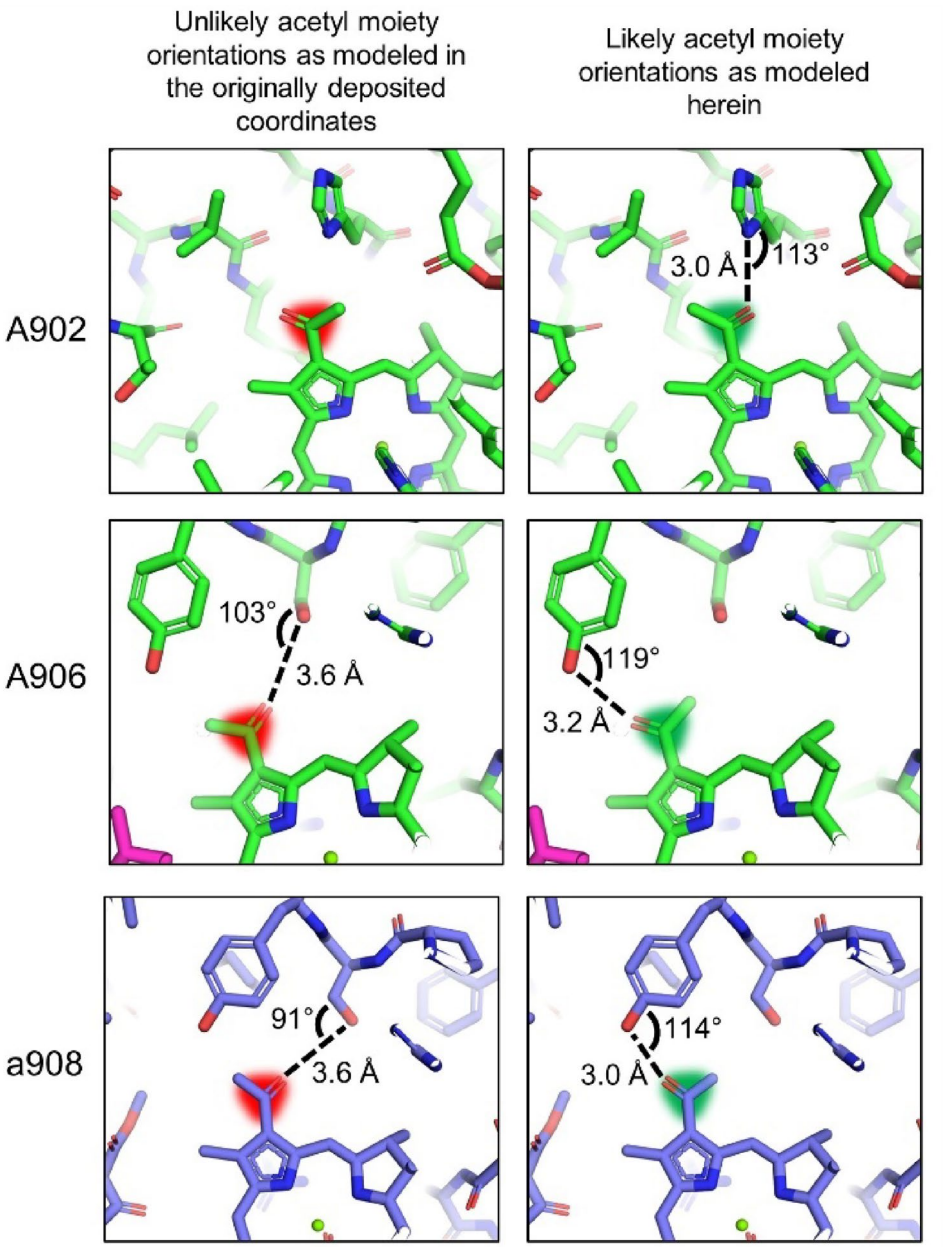

Fig. 5 Revised BChl *a* acetyl moiety orientations. The three BChl *a* sites whose acetyl moiety orientations are revised herein are shown. The left column shows the originally deposited coordinates (red glow) and the right column shows the revised orientations (green glow)

The acetyl moieties of the BChl *a* molecules in sites A906 and a908, which are related by symmetry, are also found in unlikely orientations. Although their carbonyl groups are directed toward a possible H-bond donor (PscA-Ser331), the distance and geometry are unlikely for an H-bonding interaction. Flipping their acetyl groups results in a more optimal H-bonding interaction with PscA-Tyr332 (Fig. 5). Thus, the acetyl moieties of the three BChl *a* molecules, in sites A902, A906, and a908, are most likely incorrectly modeled in the deposited coordinates. We generated an updated structure that included these changes and in which 16 of the 18 BChl *a* or Zn-BChl *a′* molecules exhibit H-bond donors to the C3 acetyl moiety. It should also be noted that all residues involved in H-bonding with the C3 acetyl moieties of BChl *a* molecules are conserved among *Chloracidobacterium* species (Supplementary Fig. 5).

The two BChl *a* molecules in sites A907 and a909, which are related by symmetry, exhibit no H-bond donors near their C3 acetyl moieties. This environment for the acetyl moiety is surprising, as all the other BChl *a* acetyl moieties have reasonable H-bonding interactions. This lack of H-bonding interactions was also suggested for one of the six Chl *b* sites, which contains a formyl moiety at its C7 position, in structures of light-harvesting complex II. In that case, the authors suggested that the sixth site could contain a mixture of chlorophyll types (Standfuss et al. 2005). We cannot rule out a similar possibility of mixed Chl *a*/BChl *a* sites for A907 and a909, but a visual inspection of their C3

positions suggests that the most likely correct assignment is BChl *a*.

Experimental cone scans and comparison with theoretical observations.

With the revised structure, we tested the following hypotheses by comparing the calculated cone scans with the experimental cone scans: (1) the C3 cone scans of Chl *a* sites exhibit a single primary peak corresponding to the position of the vinyl moiety; (2) the C3 cone scans of BChl *a* sites exhibit a two-peak profile; (3) the BChl *a* C3 cone scan at a distance of 1.23 Å exhibits similar signals for the methyl and carbonyl groups; and (4) the BChl *a* C3 cone scan at a distance of 1.57 Å exhibits a greater signal for the methyl group than for the carbonyl group. The experimental cone scans were performed on Chl *a* molecules at 1.44 Å (the expected distance of a C = C bond), and on BChl *a* molecules at 1.23 Å and 1.57 Å (the expected distances of C = O and C − C bonds, respectively) (Fig. 6). The cone angles were 120° in all scans, and the scans were sorted by the local resolution of the (B)Chl (Supplementary Table. 1).

All of the C3 cone scans of Chl *a* molecules exhibit a single primary peak for the C3 vinyl moiety. Some of the Chl *a* molecules with the highest local resolution have cone scans with either a small peak or a shoulder centered ~ 180° from the primary peak. This smaller peak may arise in part from the H-atom on the $C3^1$ atom as shown in the theoretical cone scan data (Fig. 3a, lower panel). Interestingly, we note that all of the Chl *a* molecules in the CabRC structures have their C3 vinyl moieties directed in the same orientation, at ~ 15°. In contrast to the single-peak profiles of the

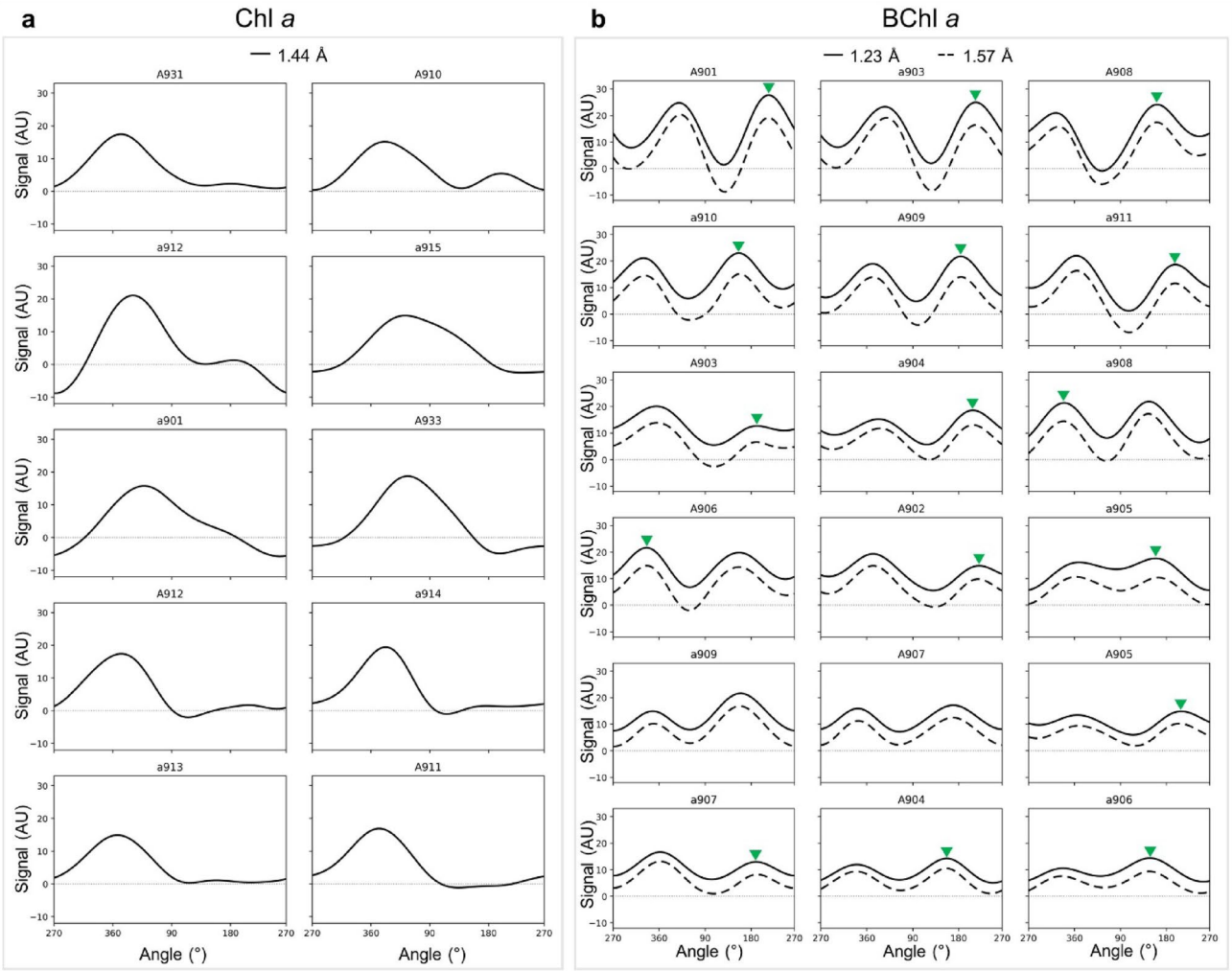

Fig. 6 Experimental cone scans of Chl *a* and BChl *a* sites. Panel **a** shows the cone scans for Chl *a*, and panel **b** shows the cone scans for Zn-BChl *a′* and BChl *a*. In **b**, the nearby H-bond donor to the C3 acetyl moiety based on the revisions described above (Figs. 4 and 5) is shown with a green arrow for each site. Note that the BChl *a* molecules in sites A907 and a909 do not exhibit nearby H-bond donors. (B)Chl sites are arranged for each panel by local resolution (Supplementary Table 1)

Chl *a* cone scans, all of the C3 cone scans of BChl *a* molecules exhibited two peaks of similar amplitude separated by ~ 180°. Thus, Chl *a* and BChl *a* are easily distinguished in the 2.2-Å resolution cryo-EM map, where a cone scan with a double-peak profile suggests the site assignment as a BChl *a* molecule and a cone scan with a single-peak profile suggests the assignment as a Chl *a* molecule. Assuming that the H-bond donor is nearest to the peak arising from the carbonyl group (green arrows in Fig. 6b), we tested the hypothesis that the carbonyl peak is less intense than the methyl peak for the cone scans at 1.23 Å and 1.57 Å. For both, there was no clear pattern of peak intensity. Thus, we conclude that the orientation of the acetyl moiety cannot be distinguished using the cone scan method at 2.2-Å resolution.

Discussion

Our data suggest that Chl *a* and BChl *a* are indeed distinguishable in an experimental cryo-EM map of ~ 2.2 Å-resolution using the cone scan method, and furthermore that these (B)Chl types may be differentiated using this method in maps with resolutions as low as ~ 3.0 Å, although this should not be taken as a strict cutoff because individual maps often differ in quality. We additionally conclude that 2.2 Å-resolution is insufficient to determine the orientation of the BChl *a* C3 acetyl moiety (i.e., to distinguish between a methyl group and a carbonyl group), which probably requires much higher resolution, at least ~ 2.0 Å. This highlights the important consideration that the ability to distinguish features in cryo-EM maps depends on the resolution of the map. Intuitively, preparing cone scans of a map at very low resolution may not be useful for determining even (B)Chl type, yet a map at much higher resolution may be useful for distinguishing even the orientation of the acetyl moiety. Note, however, that the signal contributions from charged atoms do not scale linearly with resolution in cryo-EM (Wang and Moore 2017). In low-resolution data, negative atomic charge decreases the cryo-EM map signal and positive charge increases the cryo-EM map signal, yet in high-resolution data, these effects become negligible. The data used to construct a cryo-EM map contain contributions of a gradient of resolution, from ~ 60–50 Å to the high-resolution cutoff reported (e.g., ~ 2.2 Å in the case of the CabRC structure), so the deposited cryo-EM map contains a mixture of these effects which would be challenging to deconvolute. Nonetheless, the ability to quantify the cryo-EM map corresponding to the features vital for assignment of (B)Chl type, and to compare this to theoretical expectations, is far more accurate than simply fitting the molecule into the cryo-EM by visual inspection, which is presently common practice.

A limitation of our density functional theory-derived maps is that they neglect the contribution of signals from the protein environment. In the case where high resolution is dominant, e.g., the top three graphs in Fig. 6b, the expectation that the carbonyl oxygen atom contributes a smaller peak to the scan profile than does the methyl group is met. In these high-resolution regions, the nearby H-bond donors to the carbonyl groups are sufficiently distant so as not to contribute to the corresponding cone scan peak. The situation is reversed in the case of lower local resolution, e.g., the bottom three graphs in Fig. 6b, where the smoothing of the nearby H-bond donors likely bleeds into the cone scan near the carbonyl oxygen, causing it to exhibit a peak greater than the methyl group. Thus, even a qualitative understanding of what might be expected for various map features is useful for assigning (B)Chl types.

Lastly, we wish to emphasize the necessity of identifying H-bond donors to the carbonyl oxygen atoms that frequently distinguish (B)Chl types. In the case of the CabRC analysis described here, the orientation of the acetyl moiety could not be directly determined by the cone scan method at the given resolution, but the chemical environment was easily assessed to determine this. The energetic penalty for a carbonyl oxygen atom in a hydrophobic environment is expected to be quite high, so it is unsurprising that almost every (B)Chl carbonyl oxygen atom has a nearby H-bond donor in the available structural data. We also note that if a genetic system was established for *C. thermophilum*, making mutations that abolish the H-bonding interactions to the acetyl moiety of the BChl molecules would be a possible way to investigate how the chemical environments of BChl molecules influence their spectral properties. Finally, as has been suggested for Chl *f* and Chl *a* binding (Gisriel et al. 2022a), the absence of H-bonding may lead to binding sites that can be occupied by either BChl *a* or Chl *a*; thus, it could be possible that the pigment bound to such sites might vary as a function of growth conditions or overall rates of pigment synthesis.

Conclusions

(B)Chl protein complexes are among the most cofactor-rich macromolecules found in biology, and their functions greatly depend on the (B)Chl molecules that they coordinate. The ability to derive functional insight from those structures that contain a mixture of (B)Chl types, or to use the structures for the interpretation of functional data, depends upon the accuracy of (B)Chl type assignment. To this end, theoretical calculations can assist in determining expected characteristics of different (B)Chl types in cryo-EM maps and can be subsequently used to compare against experimental data for (B)Chl type determination. For the CabRC, we have used such an analysis to show that the Chl *a* and BChl *a* molecules are correctly assigned. Although differentiating

the orientation of the BChl *a* C3 acetyl moiety is unreliable at ~ 2.2-Å resolution, identifying H-bond donation from the protein environment to the carbonyl group can be used instead. Our analysis of the CabRC system provides insight into how mixed (B)Chl systems may be modeled more accurately in the future and how similar quantitative methods can be implemented to aid in cofactor assignment in cryo-EM maps.

Supplementary Information The online version contains supplementary material available at https://doi.org/10.1007/s11120-023-01047-5.

Acknowledgements This article is dedicated to the memory of Ken Sauer. The corresponding author (G.W.B.) was introduced to photosynthesis during his postdoctoral research with Ken in 1980–1982. Research reported in this publication was supported in part by the National Institute of General Medical Sciences of the National Institutes of Health under Award Number K99GM140174 to C. J. G. The content is solely the responsibility of the authors and does not necessarily represent the official views of the National Institutes of Health. This work was also supported by Department of Energy, Office of Basic Energy Sciences, Division of Chemical Sciences grant DE-FG02-05ER15646 to G. W. B. and grant DE-SC0001423 to V.S.B. D.A.F. was also supported by the Predoctoral Program in Biophysics NIH T32 GM008283. Work in the laboratory of D.A.B was supported by grant DE-FG02-94ER20137 from the Photosynthetic Systems Program, Division of Chemical Sciences, Geosciences, and Biosciences (CSGB), Office of Basic Energy Sciences of the U. S. Department of Energy.

Author contributions CJG - wrote the main manuscript and performed research. DAF - performed research. ZL - performed research. JL - performed research. JW - performed research. DAB - directed research. VSB - directed research. GWB - directed research. All authors reviewed the manuscript.

Data availability The data are available through the supplementary information.

Declarations

Conflict of interest The authors declare that they have no conflict of interest.

References

Adams PD, Afonine PV, Bunkóczi G et al (2010) PHENIX: a comprehensive python-based system for macromolecular structure solution. Acta Crystallogr Sect D 66:213–221. https://doi.org/10.1107/S0907444909052925

Becke AD (1993) Density-functional thermochemistry. III. The role of exact exchange. J Chem Phys 98:5648–5652. https://doi.org/10.1063/1.464913

Blankenship RE (2021) Molecular Mechanisms of Photosynthesis. John Wiley & Sons, Ltd., Southern Gate

Bryant DA, Canniffe DP (2018) How nature designs light-harvesting antenna systems: design principles and functional realization in chlorophototrophic prokaryotes. J Phys B Atomic Mol Phys 51:33001. https://doi.org/10.1088/1361-6455/aa9c3c

Bryant DA, Garcia Costas AM, Maresca JA et al (2007) *Candidatus* Chloracidobacterium thermophilum: an aerobic phototrophic Acidobacterium. Science 317:523–526. https://doi.org/10.1126/science.1143236

Bryant DA, Hunter CN, Warren MJ (2020) Biosynthesis of the modified tetrapyrroles-the pigments of life. J Biol Chem 295:6888–6925. https://doi.org/10.1074/jbc.REV120.006194

Charles P, Kalendra V, He Z et al (2020) Two-dimensional ^{67}Zn HYSCORE spectroscopy reveals that a Zn-bacteriochlorophyll a′ dimer is the primary donor (P_{840}) in the type-1 reaction centers of *Chloracidobacterium thermophilum*. Phys Chem Chem Phys 22:6457–6467. https://doi.org/10.1039/C9CP06556C

Chew AGM, Bryant DA (2007) Characterization of a plant-like protochlorophyllide a divinyl reductase in green sulfur bacteria. J Biol Chem 282:2967–2975. https://doi.org/10.1074/jbc.M609730200

Ditchfield R, Hehre WJ, Pople JA (1971) Self-consistent molecular-orbital methods. IX. An extended Gaussian-type basis for molecular-orbital studies of organic molecules. J Chem Phys 54:724–728. https://doi.org/10.1063/1.1674902

Dong S, Huang G, Wang C et al (2022) Structure of the Acidobacteria homodimeric reaction center bound with cytochrome *c*. Nat Commun 13:7745. https://doi.org/10.1038/s41467-022-35460-6

Emsley P, Lohkamp B, Scott WG, Cowtan K (2010) Features and development of Coot. Acta Crystallogr Sect D 66:486–501. https://doi.org/10.1107/S0907444910007493

Frisch MJ, Trucks GW, Schlegel HE et al (2016) Gaussian 16. Gaussian Inc, Wallingford CT

Gan F, Bryant DA (2015) Adaptive and acclimative responses of cyanobacteria to far-red light. Environ Microbiol 17:3450–3465. https://doi.org/10.1111/1462-2920.12992

Gan F, Shen G, Bryant DA (2014a) Occurrence of far-red light photoacclimation (FaRLiP) in diverse cyanobacteria. Life 5:4–24. https://doi.org/10.3390/life5010004

Gan F, Zhang S, Rockwell NC et al (2014b) Extensive remodeling of a cyanobacterial photosynthetic apparatus in far-red light. Science 345:1312–1317. https://doi.org/10.1126/science.1256963

Gisriel CJ, Shen G, Kurashov V et al (2020a) The structure of Photosystem I acclimated to far-red light illuminates an ecologically important acclimation process in photosynthesis. Sci Adv 6:eaay6415. https://doi.org/10.1126/sciadv.aay6415

Gisriel CJ, Wang J, Brudvig GW, Bryant DA (2020b) Opportunities and challenges for assigning cofactors in cryo-EM density maps of chlorophyll-containing proteins. Commun Biol 3:408. https://doi.org/10.1038/s42003-020-01139-1

Gisriel CJ, Huang H-L, Reiss KM et al (2021) Quantitative assessment of chlorophyll types in cryo-EM maps of photosystem I acclimated to far-red light. BBA Adv 1:100019. https://doi.org/10.1016/j.bbadva.2021.100019

Gisriel CJ, Flesher DA, Shen G et al (2022a) Structure of a photosystem I-ferredoxin complex from a marine cyanobacterium provides insights into far-red light photoacclimation. J Biol Chem 298:101408. https://doi.org/10.1016/j.jbc.2021.101408

Gisriel CJ, Shen G, Ho M-Y et al (2022b) Structure of a monomeric photosystem II core complex from a cyanobacterium acclimated to far-red light reveals the functions of chlorophylls *d* and *f*. J Biol Chem 298:101424. https://doi.org/10.1016/j.jbc.2021.101424

Gisriel CJ, Shen G, Flesher DA et al (2023) Structure of a dimeric photosystem II complex from a cyanobacterium acclimated to far-red light. J Biol Chem 299:102815. https://doi.org/10.1016/j.jbc.2022.102815

Hariharan PC, Pople JA (1973) The influence of polarization functions on molecular orbital hydrogenation energies. Theor Chim Acta 28:213–222. https://doi.org/10.1007/BF00533485

He Z, Ferlez B, Kurashov V et al (2019) Reaction centers of the thermophilic microaerophile, *Chloracidobacterium thermophilum* (Acidobacteria) I: biochemical and biophysical characterization. Photosynth Res 142:87–103. https://doi.org/10.1007/s11120-019-00650-9

Hehre WJ, Ditchfield R, Pople JA (1972) Self—consistent molecular orbital methods. XII. Further extensions of Gaussian—Type basis sets for use in molecular orbital studies of organic molecules. J Chem Phys 56:2257–2261. https://doi.org/10.1063/1.1677527

Kato K, Shinoda T, Nagao R et al (2020) Structural basis for the adaptation and function of chlorophyll *f* in photosystem I. Nat Commun 11:238. https://doi.org/10.1038/s41467-019-13898-5

Kleywegt GJ, Jones TA (1994) Halloween ... masks and bones. In: Bailey, S., Hubbard, R. & Waller D (ed) Proceedings of the CCP4 Study Weekend: From First Map to Final Model. SERC Daresbury Laboratory, Daresbury, U.K., pp 59–66

Kühlbrandt W (2014) The resolution revolution. Science 343:1443–1444. https://doi.org/10.1126/science.1251652

Sievers F, Wilm A, Dineen D et al (2011) Fast, scalable generation of high quality protein multiple sequence alignments using Clustal Omega. Mol Syst Biol 7:1–6

Standfuss J, Terwisscha van Scheltinga AC, Lamborghini M, Kühlbrandt W (2005) Mechanisms of photoprotection and nonphotochemical quenching in pea light-harvesting complex at 2.5 Å resolution. EMBO J 24:919–928. https://doi.org/10.1038/sj.emboj.7600585

Strain HH, Manning WM (1942) Chlorofucine (chlorophyll γ), a green pigment of diatoms and brown algae. J Biol Chem 144:625–636. https://doi.org/10.1016/S0021-9258(18)72486-1

Strain HH, Manning WM, Hardin G (1943) Chlorophyll *c* (chlorofucine) of diatoms and dinoflagellates. J Biol Chem 148:655–668. https://doi.org/10.1016/S0021-9258(18)72267-9

Tank M, Bryant DA (2015) *Chloracidobacterium thermophilum* gen. nov., sp. nov.: An anoxygenic microaerophilic chlorophotoheterotrophic acidobacterium. Int J Syst Evol Microbiol 65:1426–1430. https://doi.org/10.1099/ijs.0.000113

Tsukatani Y, Romberger SP, Golbeck JH, Bryant DA (2012) Isolation and characterization of homodimeric type-I reaction center complex from *Candidatus* Chloracidobacterium thermophilum, an aerobic chlorophototroph. J Biol Chem 287:5720–5732. https://doi.org/10.1074/jbc.M111.323329

van de Meent EJ, Kobayashi M, Erkelens C et al (1991) Identification of 8^1-hydroxychlorophyll *a* as a functional reaction center pigment in heliobacteria. Biochim Biophys Acta Bioenerg 1058:356–362. https://doi.org/10.1016/S0005-2728(05)80131-8

Wang J, Moore PB (2017) On the interpretation of electron microscopic maps of biological macromolecules. Protein Sci 26:122–129. https://doi.org/10.1002/pro.3060

Winn MD, Ballard CC, Cowtan KD et al (2011) Overview of the CCP4 suite and current developments. Acta Crystallogr Sect D 67:235–242. https://doi.org/10.1107/S0907444910045749

Zill JC, He Z, Tank M et al (2018) ^{15}N photo-CIDNP MAS NMR analysis of reaction centers of *Chloracidobacterium thermophilum*. Photosynth Res 137:295–305. https://doi.org/10.1007/s11120-018-0504-1